SEMARAK ILMU PUBLISHING

Journal of Advanced Research in Applied Sciences and Engineering Technology

Journal homepage:
https://semarakilmu.com.my/journals/index.php/applied_sciences_eng_tech/index
ISSN: 2462-1943

Novel Lightweight Hydraulic Integration Methodology for Robotic Applications

M. El Asswad[1], A. Abdellatif[2,*], S. Alfayad[1], K. Khalil[1,3]

[1] IBISC, Université d'Évry Paris-Saclay, 91020 Evry, France
[2] Mechanical Engineering Department, Arab Academy for Science, Technology and Maritime Transport, Sheraton branch, 11736 Cairo, Egypt
[3] ECAM-Rennes, Laboratoire Matériaux Mécanique, Campus de Kerlann, 35170 Bruz, Rennes, France

ARTICLE INFO

Article history:
Received 20 December 2023
Received in revised form 5 June 2024
Accepted 13 June 2024
Available online 31 July 2024

Keywords:

Hydraulic integration; humanoid robots; HYDROïD robot; assistive devices; composite materials; additive manufacturing

ABSTRACT

Hydraulic integration is one of the novel technologies in the field of robotics and assistive devices. Researchers have applied recent technologies starting from non-conventional machining methodologies and ending with additive manufacturing of metals. However, those methodologies have several drawbacks related to the cost, time, and robot weight. This motivates the research of new methodologies toward developing compact, cost-effective, and lightweight hydraulic integrated robotics mechanisms. This paper presents a novel methodology for fabricating hydraulically integrated parts by using lightweight and high-strength materials. The proposed materials, fabrication steps and the obtained results are thoroughly discussed. Silicon pipes are used for building the network of internal passages. This network is built inside a 3D-printed mould which is designed accordingly. A theoretical study is conducted for the newly manufactured hydraulic parts to define the design parameters and the working pressure at which the manufactured parts can withstand in addition to stresses and deformations analysis. The theoretical results are validated using finite element modelling (FEM) and experimental testing. The simulation results were consistent with the FEM results and the experimental results by 95% and 90% respectively. The proposed methodology is cheap and simple to implement in fabrication. Hence, this methodology can be used to fabricate hydraulic integrated components in hydraulically actuated humanoid robots successfully.

1. Introduction

In the modern world, more research is needed to create humanoid robots for use in industrial processes, entertainment, or research [1-3]. Some researchers have developed humanoid robots that are dedicated to entertainment purposes such as reception duties in hotels and airports, serving people in restaurants or even helping elderly people in hospitals and homes [4,5]. Humanoids are mainly actuated using electrical or hydraulic actuators. Normally, electrically actuated robots are preferred due to their control simplicity and low initial cost. Examples of electrically actuated robots

* *Corresponding author.*
E-mail address: a_abdellatif@aast.edu

https://doi.org/10.37934/araset.49.2.102117

include ARMAR-6 [6], HRP-5P [7] and WABIAN-2LL [8]. However, this type of actuation is also characterized by its heavy mechanical couplings. These couplings are needed to provide the necessary torques and velocities to achieve high dynamic activities that are required by humanoids [9,10].

Recently, several Humanoid robotics researchers have used hydraulic actuation in humanoid robots to carry out dynamic and dexterous tasks like Tae-mu [11], Atlas [12], HYDROïD [13] and WLR-II [14]. Generally, hydraulic actuation is characterized by its high torque to volume ratio, power density and high precision [15]. However, hydraulically actuated humanoid robots lack safe interaction with human beings due to their high mass/inertia in addition to the possibility of hydraulic leakage due to the presence of hydraulic pipes or hoses.

Consequently, several researchers tried to enhance hydraulic actuation with novel ideas like the introduction of hydraulic integration technology for humanoid robots like Atlas, HYDROïD and HyQmax [16]. This feat provides more system compactness and decreases the time of assembly and motion flexibility. Additionally, by eliminating the hydraulic piping system, the robot gains more morphology and social acceptance. Hydraulic integration technology has been carried out by several fabrication processes. Alfayad *et al.,* [17] has developed the hydraulic integrated HYDROïD robot using conventional machining technologies such as electric discharging. He also produced an integrated electrohydraulic actuator [18] for joint actuation. Boston Dynamics [19] has used the additive manufacturing of metals for their humanoid robot Atlas. Moog and IIT [20,21] have produced their integrated hydraulic actuator ISA 5 intended for their quadruped robot HYQ using 3D printing of titanium.

Hydraulic integration is also used in the manufacturing of assistive devices and exoskeletons. Sun *et al.,* [22] presented a novel hydraulic actuating system (HAS) which was based on an electric-hydrostatic actuator for a hydraulic lower limb exoskeleton. Each HAS contained an electric servo motor, a high-speed micro pump, an oil tank, and other components into a module. Experiments of trajectory tracking, and human-exoskeleton interaction are carried out, which demonstrate that the total weight of the HAS in the robot is reduced by about 40%, and the power density is increased by almost 1.6 times compared with the previous prototype.

Another research effort was done by Lee *et al.,* [23] in which he produced a new electro-hydraulic actuator (EHA) system to be used with a lower limb exoskeleton. The EHA prototype contains of a hydraulic pump, an electric motor, a hydraulic actuator, and a hydraulic manifold to house the hydraulic valves. Position and force control experiments were done to enable the exoskeleton to imitate the required gait cycle while monitoring the flow rate and pulsation. To control the actuator, sliding mode controller (SMC) is applied and compared with the proportional integral derivative (PID) controller.

Despite the previous research efforts, each of these mentioned fabrication processes has its drawbacks. Advanced machining process, for example, electric discharging, suffers from high cost and long fabrication time [24]. Moreover, the produced component necessitates post procedures such as surface finish and soldering, which increases the price of the produced part. Secondly, the additive manufacturing of metals is expensive [25] and is expected to be used for limited space. Furthermore, high printing precision is obtained when the integrated component has a constant cross-section, which isn't true for most cases of hydraulic integrated parts. Consequently, it is important to develop an adaptable methodology for fabricating hydraulic integrated robot components, which uses high strength-to-weight ratio materials, resolves the complexity, and reduces the cost of manufacturing. This paper presents a new methodology for fabricating hydraulic integrated components with high strength, low cost, and a simple manufacturing process.

2. Problem Statement

The fabrication of a hydraulic integrated part is a complex and expensive process. Figure 1 gives an example of a hydraulic integrated part used in HYDROïD robot arm. It contains 14 passages in several directions, for which some of which measures 100 mm in length and 3 mm in diameter. It would be difficult to fabricate this part using classical machining (pressing or turning) due to the length and small dimensions of the passages. So, electric discharging is used to do 100 mm holes of small diameters (starting from 3 mm and up to 10 mm). Then, laser welding is used to close the unnecessary openings. However, this method is time-consuming and requires later post-processes such as surface finish where the welder is applied. This would inherently increase the price of the hydraulic integrated part and the mechanism overall. Additionally, electric discharging would, in some cases, alter the mechanical properties of the part material due to the high temperature effect [26,27].

Normally, additive manufacturing of metals can be used for fabricating this part [28]. Two recent technologies could be used to accomplish this: selective laser sintering (SLS) and electron beam melting (EBM). SLS technology has limitations in terms of part dimensions/shape related to printing accuracy. The high accuracy of printing is obtained when the part has a constant cross-section, which isn't the case for the shown part because the passages are not symmetrically distributed. Also, due to the small dimensions of the holes, it would be difficult to remove the powder metallic support. This is also applicable to the EBM technology which is very limited in terms of dimensions of the parts [29]. Furthermore, both technologies should be followed by heat treatment and surface finish, due to the fragility of the produced part. Moreover, additive manufacturing of metals is still a relatively expensive process which affects the price of the whole process [25]. Consequently, it is important to find a new methodology for fabricating hydraulic integrated parts which could be simple, relatively cheap and uses lightweight and high strength materials such as composites.

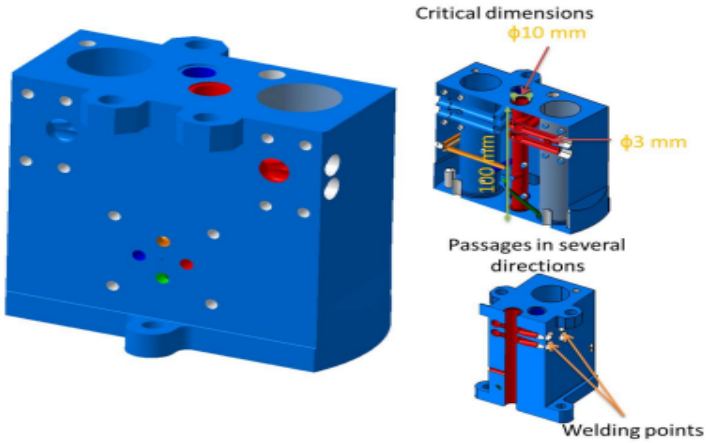

Fig. 1. Example of a hydraulic integrated part

3. Proposed Solution

The novel methodology presented in this paper proposes the usage of silicon pipes for building the network of internal passages. This network is built inside a 3D-printed mould, designed accordingly. All the hydraulic components, including the hydraulic adapter, are directly integrated into the printed mould. In addition, a 3D-printed elbow is used to connect two perpendicular silicon pipes. Figure 2 gives an example of the setup of the proposed methodology. Thus, the proposed

methodology consists of 6 steps: mould design, 3D-printing the mould, installing internal passages and some other accessories, adding resin or random carbon fibre-reinforced polymers, removing the mould, and finishing the parts. First, the mould is designed using CAD software, before it is fabricated using the appropriate 3D printing technology. Second, silicone tubes are installed to resemble the integrated passages of the old parts. Third, the random carbon fibre material is prepared, and added to the silicone pipes network, to match the requirements of mechanical properties. Moreover, the mould is removed to get the moulded part.

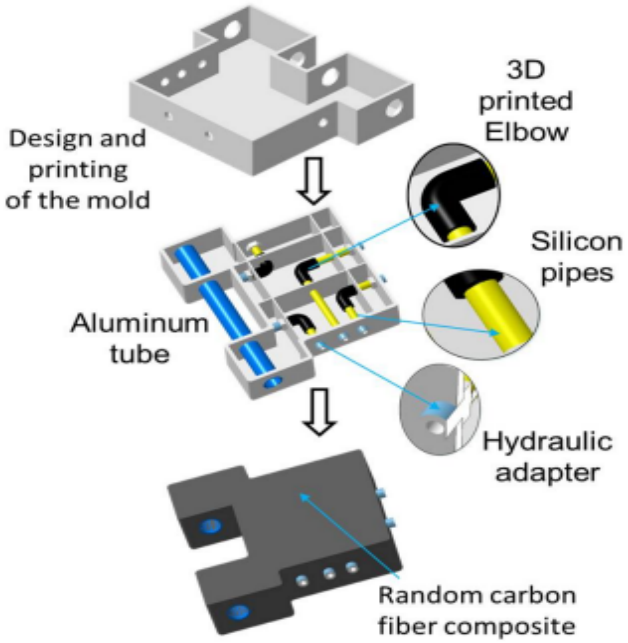

Fig. 2. Representation of the proposed methodology

4. Theoretical Calculations

In this section, the main issue is to define the validated design parameters and the working pressure at which the part can resist the stresses. The main design parameters that are included are the internal diametric ratio R_i and the external diametric ratio R_o. To do that, the applied theory is the multi-layer theory, in which the internal layer is the silicone tube, while the external layer is the random fibre composite reinforcement (Figure 3).

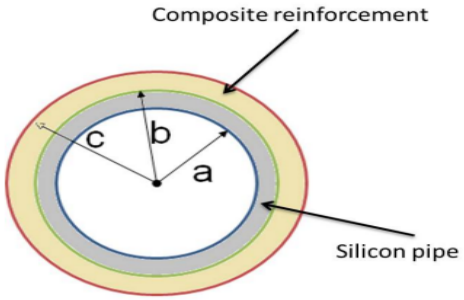

Fig. 3. Geometrical Presentation of the multi-layer tube: a) internal diameter of the internal layer, b) the internal diameter of the outer layer and c the outer diameter of the outer layer

To find these design parameters, the classical elasticity theory of multi-layer thick-walled cylinders is used [30]. The elasticity material parameters of the internal and the external layers are designated as E_i Young modulus of the internal layer, ν_i the Poisson ratio of the internal layer, E_o the Young modulus of the external layer and ν_o is the Poisson ratio of the external layer. Thus, due to the internal pressure P_i, an interface radial stress P_f is produced. Applying the theory, P_f can be calculated as follows [31]:

$$P_f = \frac{2P_i}{\left[\left(R_i^2+1-\nu_i\right)+\frac{E_i}{E_o}\left(\left(R_i^2-1\right)\frac{R_o^2+1}{R_o^2-1}+\nu_o\right)\right]} \quad (1)$$

Where $R_i = \frac{b}{a}$ and $R_o = \frac{c}{a}$ are the diametric ratio of the internal and the external layers respectively.

However, the Young modulus of the silicone tube E_i (1-3 MPa) is very small compared to the composite Young modulus (at least 20 GPa). Thus, the ratio E_i/E_o tends to 0 and P_f can be simplified to the following expression:

$$P_f = \frac{2P_i}{\left(R_i^2+1-\nu_i\right)} \quad (2)$$

Then, the maximum hoop stress and radial strain at the internal layer could be expressed in Eq. (3) and Eq. (4) according to Lame's equations as follows:

$$\sigma_{him} = \frac{P_i}{\left(R_i^2-1\right)}\left(1+R_i^2\right) - \frac{2P_iR_o^2}{R_i^2-1} \quad (3)$$

$$\epsilon_r = \frac{1}{E_i}\frac{\left(P_i-P_fR_i^2\right)(\nu_i-1)+R_i^2(P_f-P_i)(\nu_i+1)}{1-R_i^2} \quad (4)$$

According to the simplification, the hoop stresses σ_{him} and the interference pressure P_f are independent of the outer layer material characteristics. It depends only on the thickness of the reinforcement.

5. Simulation Analysis

To apply the theory, a simulation study on three different types of silicone tubes: shore 70 silicone tube, shore 60 silicone tube and shore 50 silicone tube, has been carried out. For each category, the hoop stresses and the radial deformation are plotted against the internal diametric ratio R_i and the applied pressure P_i, for three different values of the design parameter R_o: 1.5, 2 and 2.5. The applicable zones, which verify the acceptable strength and deformation of the silicone tube, are plotted in the red area for each category. The characteristics of the chosen silicone tubes for the case studies are mentioned in the Table 1.

Table 1
Different characteristics of the chosen silicone tubes: Acceptable stress σ_{acc} (MPa), acceptable deformation ε_{acc} (%), young modulus E_i (MPa)

Silicone category	σ_{acc} (MPa)	ε_{acc} (%)	E_i (MPa)
shore 70	10	320	2.86
shore 60	8.9	429	1.6
shore 50	9.3	900	1.31

5.1 Stress Analysis

The following 3D graphs give the study of the internal hoop stresses σ_{him} as a function of the internal diametric ratio Ri and the applied pressure P_i. It is given for the 3 categories of the silicone tubes: shore 50, shore 60 and shore 70 silicone tubes represented respectively in figures Figure 4, Figure 5 and Figure 6. In addition, the 2D graphs represent the zone of acceptable values (in red) for the 3 types of silicone.

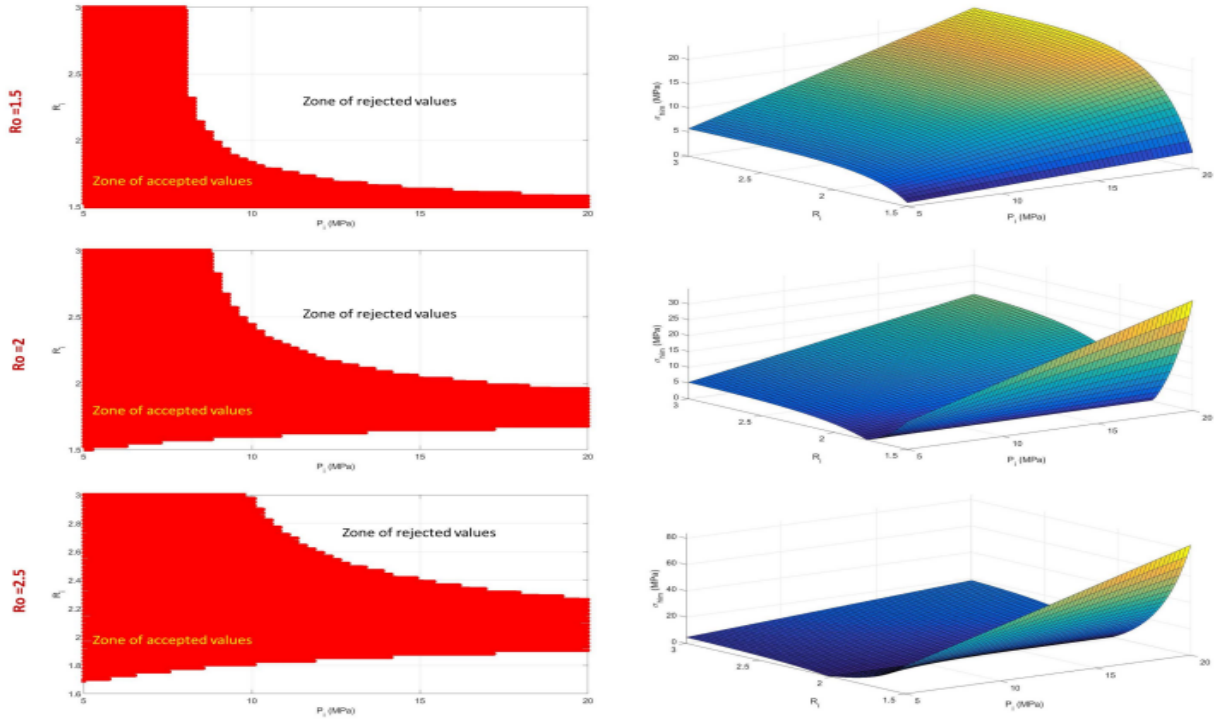

Fig. 4. 3D and 2D representations of the hoop stress σ_{him} variations for shore 50 silicone tube as a function of the internal diametric ratio R_i and the applied pressure P

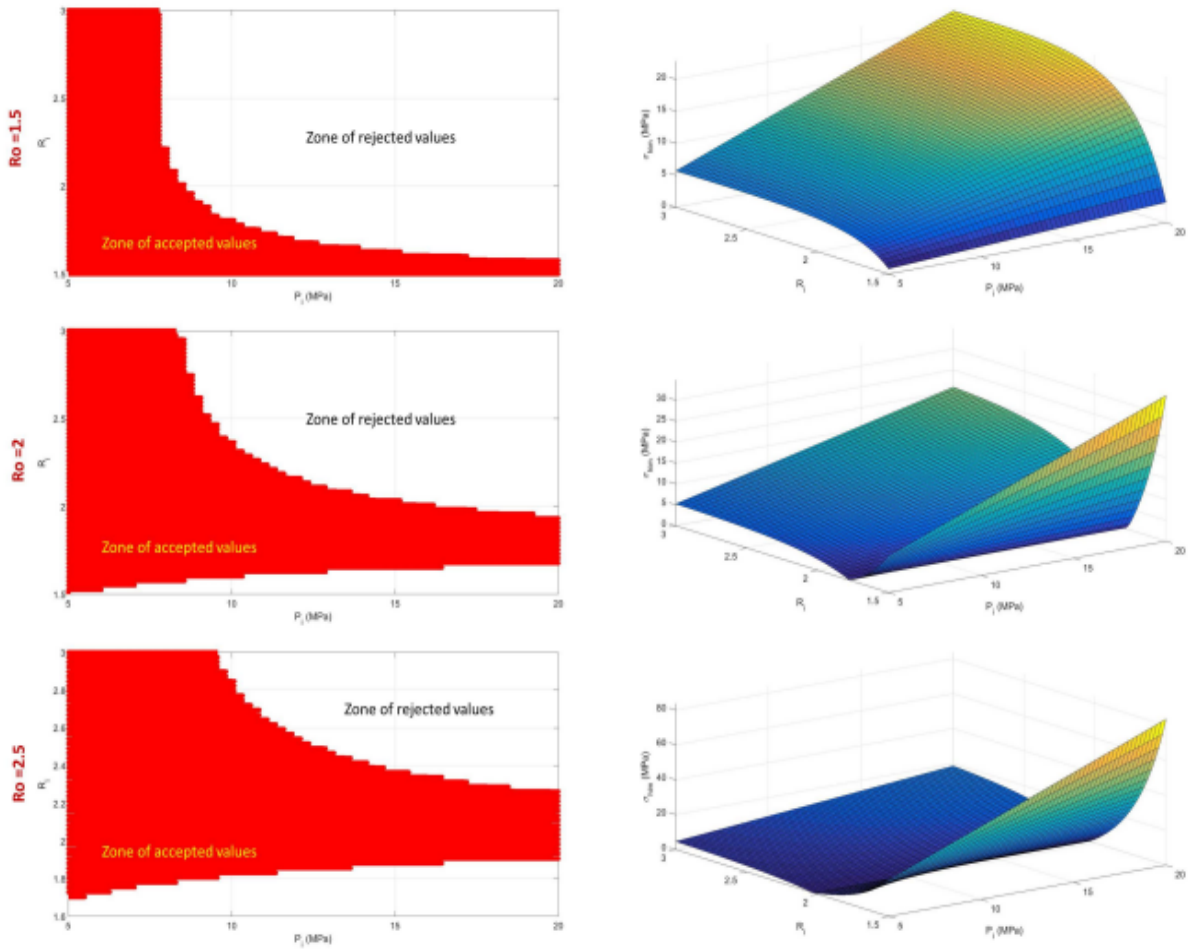

Fig. 5. 3D and 2D representations of the hoop stress σ_{him} variations for shore 60 silicone tube as a function of the internal diametric ratio R_i and the applied pressure P_i

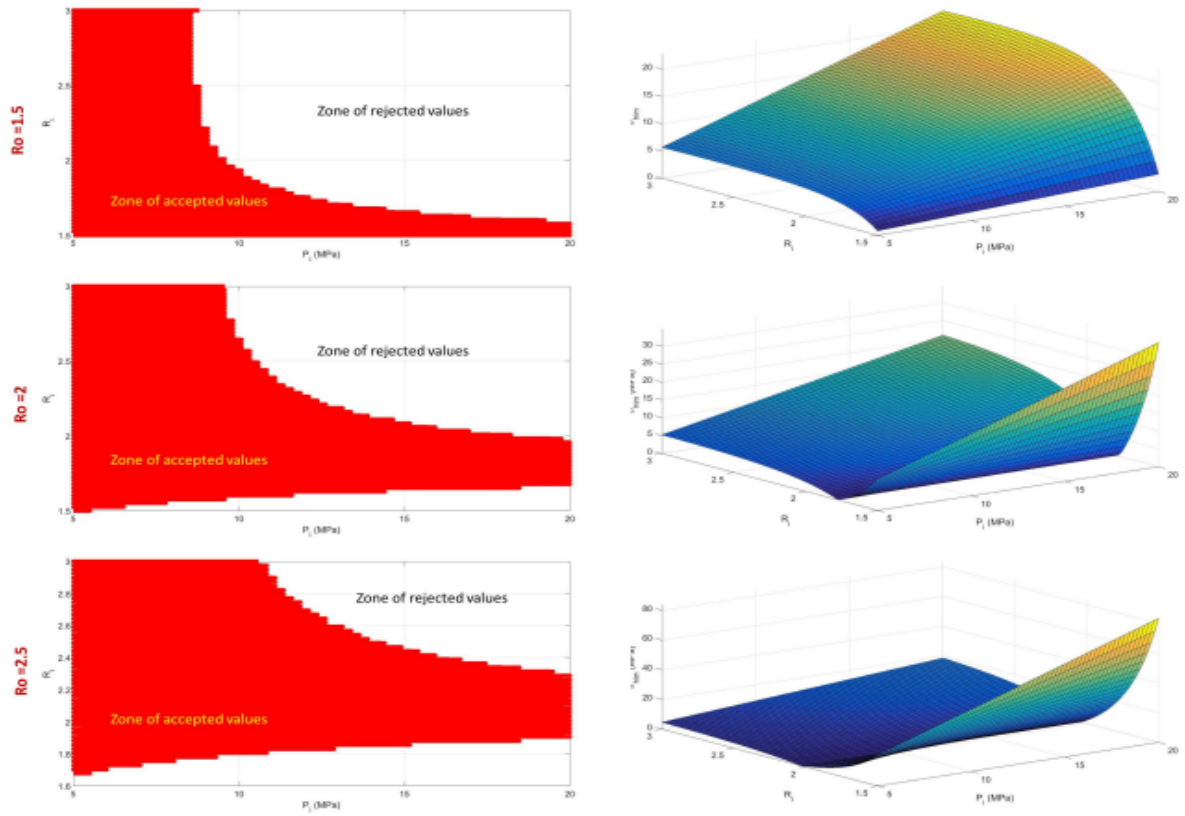

Fig. 6. 3D and 2D representations of the hoop stress σ_{him} variations for shore 70 silicone tube as a function of the internal diametric ratio R_i and the applied pressure P_i

According to the curves, the zone of the acceptable values of R_i and P_i increases when the outer diametric ratio R_o increases. For example, for P_i = 15 MPa, the R_i ranges from 1.8 to 2.4 for R_o=2.5 while it ranges from 1.7 to 2.2 for R_o=2, for shore 70 silicone tube. In addition, it is noticed that for R_o=2 and R_o=2.5, there is a zone of minimal hoop stresses, while it isn't the same for R_o=1.5. Thus, the outer diametric ratio R_o has an important impact on minimizing the internal hoop stresses σ_{him} regardless of the reinforcement material type. On the other hand, the acceptable zone slightly increases with the increase of the shore hardness of the silicone tube. For example, for shore hardness 60 silicone tube and at R_o=2.5, the internal diametric ratio R_i varies from 1.95 to 2.4 at an applied pressure P_i=15 MPa, while it slightly increases for shore 70 silicone tube, with a range from 1.8 to 2.5. This is because the three categories have approximately equal acceptable strength. Thus, the variation of the silicone material type has a slight impact on the area of the acceptable zones.

5.2 Deformation Analysis

The following 3D graphs give the study of the radial deformation ε_r as a function of the internal diametric ratio R_i and the applied pressure P_i. It is given for the 3 categories of the silicone tubes: shore 50, shore 60 and shore 70 silicone tubes represented respectively in Figure 7, Figure 8 and Figure 9. In addition, the 2D graphs represent the zone of acceptable values (in red) for the 3 types of silicone.

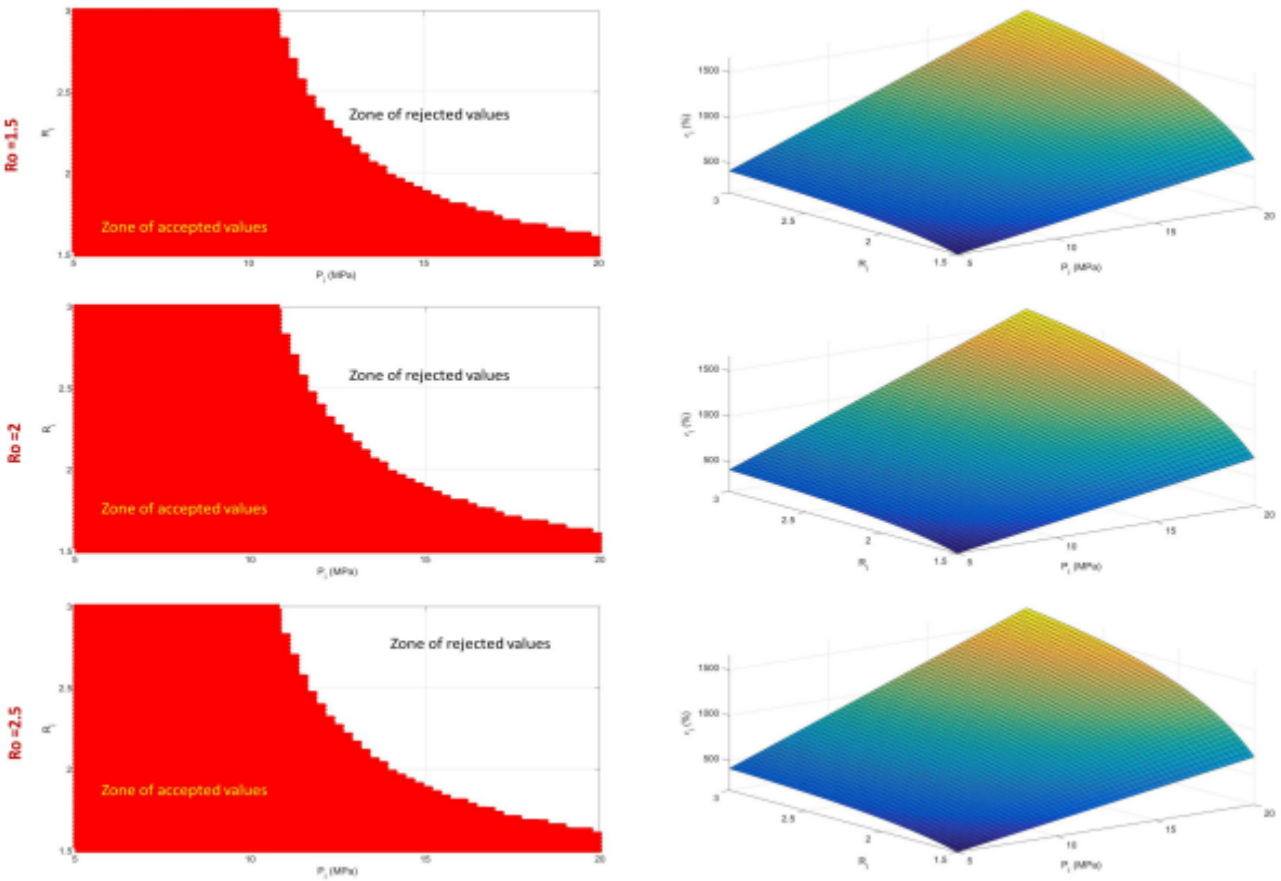

Fig. 7. 3D and 2D representations of the radial deformation ε_r variations for shore 50 silicone tube as a function of the internal diametric ratio R_i and the applied pressure P_i

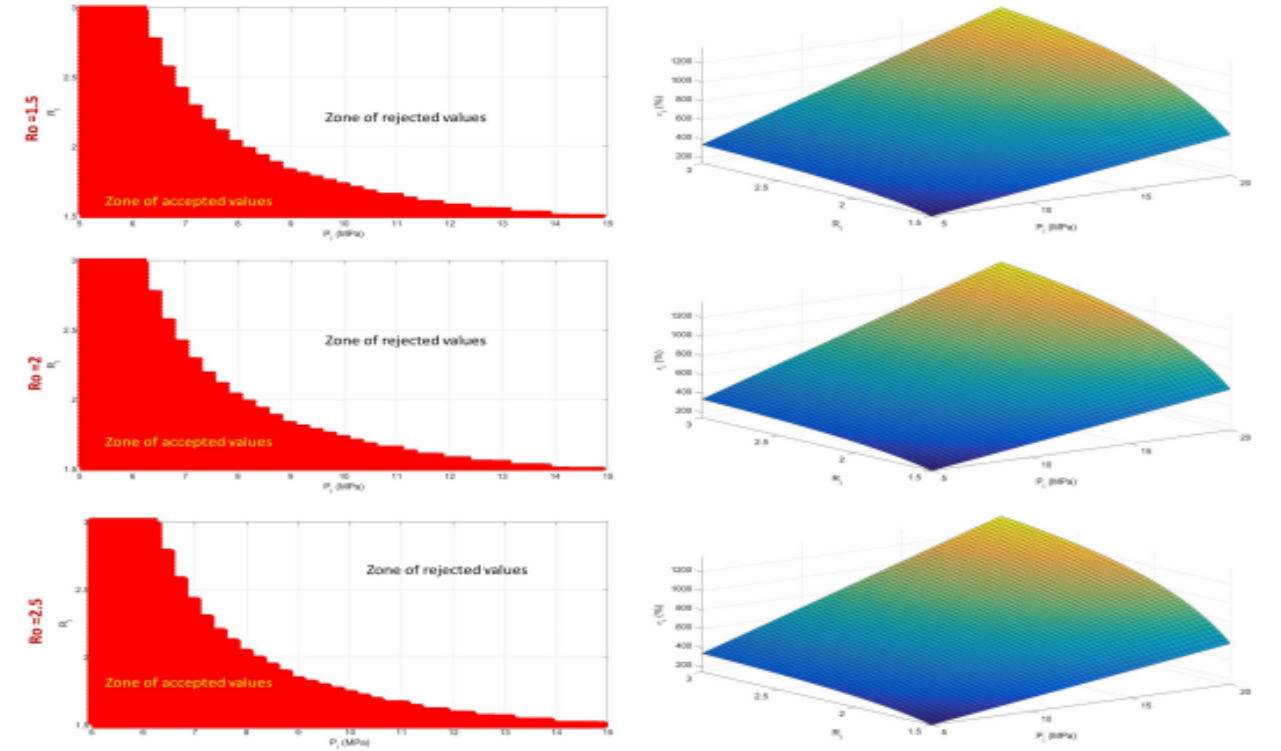

Fig. 8. 3D and 2D representations of the radial deformation ε_r variations for shore 60 silicone tube as a function of the internal diametric ratio R_i and the applied pressure P_i

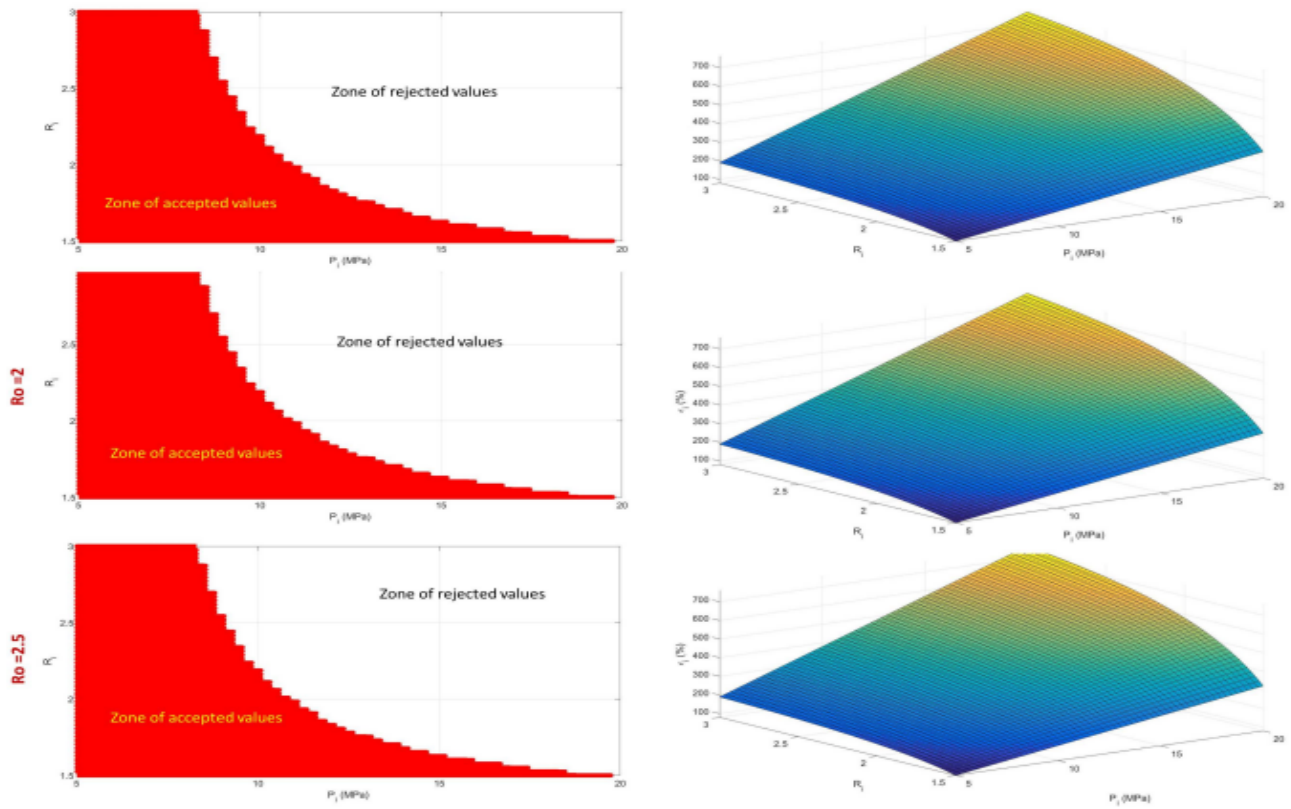

Fig. 9. 3D and 2D representations of the radial deformation ε_r variations for shore 70 silicone tube as a function of the internal diametric ratio R_i and the applied pressure P_i

According to the previous curves, the zone of the acceptable values of R_i and P_i doesn't change when the outer diametric ratio R_o increases. for example, for P_i = 12 MPa, the R_i ranges from 1.5 to 1.75 for R_o=2.5, 2 and 1.5 while it ranges from 1.7 to 2.2 for R_o=2, for shore 60 silicone tube. Thus, the outer diametric ratio R_o has no impact on minimizing the radial deformation ε_r regardless of the reinforcement material type. On the other hand, the acceptable zone increases with the decrease of the shore hardness of the silicone tube from 70 to 50. For example, for shore hardness 60 silicone tube and at R_o=2.5, the internal diametric ratio R_i varies from 1.5 to 1.75 at an applied pressure P_i=12 MPa, while it inherently increases for shore 50 silicone tube, with a range from 1.5 to 2.45. This is because the three categories have very different acceptable deformation before the break and Young modulus. Thus, the variation of the silicone material type has an important impact on the volume of the acceptable zones.

5.3 Finite Element Modelling

A 3D model of a multi-layer tube is built into simulation software to validate the theoretical results. A brick element for meshing is used, where the mesh size is 0.7 mm. The contact between the silicone and the reinforcement layers is rough solid-to-solid contact (Figure 10). The inner surface of the internal layer is subjected to discrete values of pressure P_i=50, 100, 150 and 200 bar. The model is tested for different dimensions of the silicone tube and the reinforcement tube and for three types of silicone material: shore 50, 60 and 70 silicone tubes. For all cases, the silicone tube inner diameter is chosen as r_i=1.5 mm.

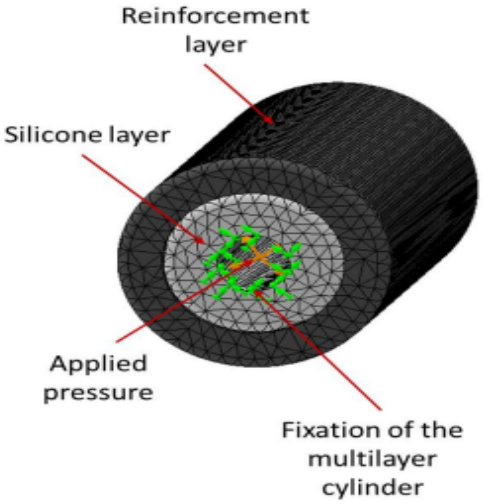

Fig. 10. FEM model of the multi-layer tube

The following tables summarize the cases for which the stresses and the strains of the multi-layer are evaluated using the FEM; the evaluated stresses and strains are compared with those found by the theoretical results. Then, the error is calculated to estimate the confidence of the finite element model. The following 3 tables give the stresses and the strains for R_o=1.5, R_i=1.5, 2, 2.5 and for each material at different applied pressures.

According to these tables, the difference between the theoretical results and the finite element model method varies according to the case and to the calculated parameter (stress or strain). The average error in stress calculations is around 5% for R_i=1.5, 4% for R_i=2 and 6% for R_i=2.5. While for the strain calculations, the average error is 9% for R_i=1.5, 17% for R_i=2 and 4% for R_i=2.5. These results give an overall average of 5% error between the theoretical and the FEM values, which means that the theory is 95% coherent with the proposed model.

Table 2
Cases used in the finite element model

Material	R_i=50			R_i=100			R_i=150			R_i=200		
	R_i=1.5	R_i=2	R_i=2.5	R_i=1.5	R_i=2	R_i=2.5	R_i=1.5	R_i=2	R_i=2.5	R_i=1.5	R_i=2	R_i=2.5
3xShore70	R_o=1.5	R_o=1.5	R_o=1.5	R_o=1.5	R_o=1.5	R_o=1.5	R_o=1.5	R_o=1.5	R_o=1.5	R_o=1.5	R_o=1.5	R_o=1.5
	R_o=2	R_o=2	R_o=2	R_o=2	R_o=2	R_o=2	R_o=2	R_o=2	R_o=2	R_o=2	R_o=2	R_o=2
	R_o=2.5	R_o=2.5	R_o=2.5	R_o=2.5	R_o=2.5	R_o=2.5	R_o=2.5	R_o=2.5	R_o=2.5	R_o=2.5	R_o=2.5	R_o=2.5
3xShore60	R_o=1.5	R_o=1.5	R_o=1.5	R_o=1.5	R_o=1.5	R_o=1.5	R_o=1.5	R_o=1.5	R_o=1.5	R_o=1.5	R_o=1.5	R_o=1.5
	R_o=2	R_o=2	R_o=2	R_o=2	R_o=2	R_o=2	R_o=2	R_o=2	R_o=2	R_o=2	R_o=2	R_o=2
	R_o=2.5	R_o=2.5	R_o=2.5	R_o=2.5	R_o=2.5	R_o=2.5	R_o=2.5	R_o=2.5	R_o=2.5	R_o=2.5	R_o=2.5	R_o=2.5
3xShore50	R_o=1.5	R_o=1.5	R_o=1.5	R_o=1.5	R_o=1.5	R_o=1.5	R_o=1.5	R_o=1.5	R_o=1.5	R_o=1.5	R_o=1.5	R_o=1.5
	R_o=2	R_o=2	R_o=2	R_o=2	R_o=2	R_o=2	R_o=2	R_o=2	R_o=2	R_o=2	R_o=2	R_o=2
	R_o=2.5	R_o=2.5	R_o=2.5	R_o=2.5	R_o=2.5	R_o=2.5	R_o=2.5	R_o=2.5	R_o=2.5	R_o=2.5	R_o=2.5	R_o=2.5

Table 3
Evaluated stress σ_{him}(MPa) and strain ε_r(%) calculated by theoretical and FEM methods for internal diameter R_i=1.5

Material		P_i=50		P_i=100		P_i=150		P_i=200	
		σ_{him}(MPa)	ε_r(%)	σ_{him}(MPa)	ε_r(%)	σ_{him}(MPa)	ε_r(%)	σ_{him}(MPa)	ε_r(%)
2xShore70	theoretical	0.83456	74	1.6427	148	2.376	222	3.186	296
	FEM	0.7966	80	1.607	162	2.40816	243.6	3.6	321
2xShore60	theoretical	0.83456	143.5	1.6427	289.5	2.376	435	3.186	616
	FEM	0.7966	158	1.607	295	2.40816	454	3.6	574
2xShore50	theoretical	0.83456	175	1.6427	354	2.376	523	3.186	701.3
	FEM	0.7966	195	1.607	390	2.40816	586	3.6	780

Table 4
Evaluated stress σ_{him}(MPa) and strain ε_r(%) calculated by theoretical and FEM methods for internal diameter R_i=2

Material		P_i=50		P_i=100		P_i=150		P_i=200	
		σ_{him}(MPa)	ε_r(%)	σ_{him}(MPa)	ε_r(%)	σ_{him}(MPa)	ε_r(%)	σ_{him}(MPa)	ε_r(%)
2xShore70	theoretical	5.226	118	10.41	328	15.46	359	20.65	478
	FEM	5.486	145	10.99	295	15.68	443	21.23	584
2xShore60	theoretical	5.226	218	10.41	436	15.4	655	20.65	861
	FEM	5.48	261	10.99	526	15.68	792	21.23	1045
2xShore50	theoretical	5.22	268	10.41	537	15.4	805	20.65	1073
	FEM	5.48	319	10.99	643.3	15.68	952	21.23	1276

Table 5
Evaluated stress σ_{him}(MPa) and strain ε_r(%) calculated by theoretical and FEM methods for internal diameter R_i=2.5

Material		P_i=50		P_i=100		P_i=150		P_i=200	
		σ_{him}(MPa)	ε_r(%)	σ_{him}(MPa)	ε_r(%)	σ_{him}(MPa)	ε_r(%)	σ_{him}(MPa)	ε_r(%)
2xShore70	theoretical	5.7	175	11.4	352	17.2	504	22.68	700
	FEM	6.1	165	11.95	331	18.22	496	24.4	728
2xShore60	theoretical	5.7	312	11.4	630	17.2	945	22.68	1250
	FEM	6.1	293	11.95	593	18.22	910	24.4	1187
2xShore50	theoretical	5.7	377	11.4	760	17.2	1144	22.68	1508
	FEM	6.1	365	11.95	729	18.22	1094	24.4	1458

6. Experimental Validation

To validate the new methodology and approve the obtained theoretical results, composite material samples are fabricated and tested under pressure. The chosen silicone tube is shore 60, with 4 mm internal diameter, 1-, 2- and 3-mm thickness, which gives an inner diametric ratio R_i = 1.5, 2 and 2.5 in correspondence with the carried out theoretical and FEM procedures. The added composite reinforcement layer is random carbon fibre mixed with epoxy with a fibre aspect ratio equal to 10 % and external diameter fixed to 15 mm, which gives an outer diametric ratio R_o= 1.5, 2 and 2.5. Thus, the tested samples are shore 60 and milled carbon fibre/epoxy composites with three categories of dimensions: R_i, R_o = 1.5, 2.5, R_i, R_o = 2, 2 and R_i, Ro = 2.5, 1.5 respectively. 5 samples are fabricated of each category.

To fabricate these samples, a mould containing three samples (1 of each category) is designed and fabricated using 3D-printed plastic. Then, three tubes of each category and connected to hydraulic adapters, are installed inside the mould. Then, milled carbon fibre/epoxy composite is added as a reinforcement layer (Figure 11a). To remove the voids from the moulded composites, the

degassing chamber is used (Figure 11b). The resin filled with carbon fibre is placed inside the chamber at a vacuum -0.4 mbar for 15 min before it is added to the mould. Then, the moulded part with the composite is placed itself inside the chamber to make sure almost all the voids are eliminated.

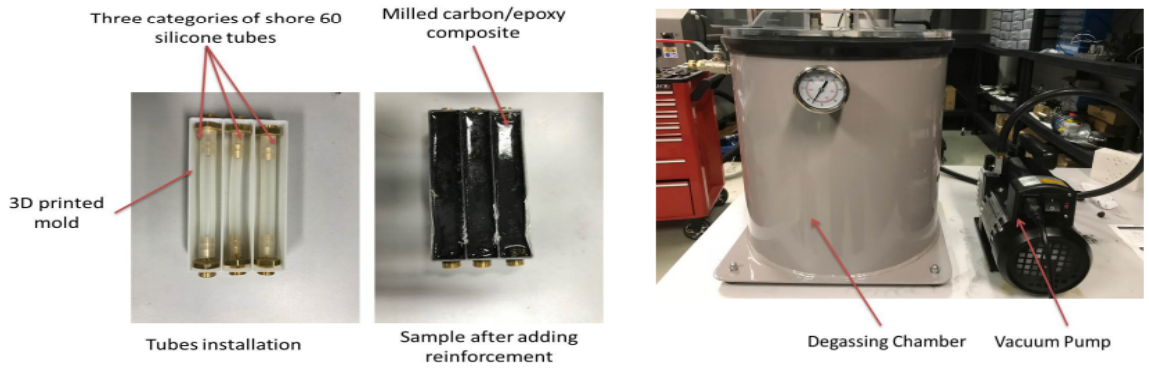

Fig. 11. (a) FEM model of the multi-layer tube (b) Degassing chamber used for void removal

Each sample is then placed at a hydraulic test bench with chip-in oil pressure sensors, placed in a manifold block at the inlet and outlet of the servo-valve (Figure 12). The samples are tested under pressure levels lower than or equal to the already calculated maximum pressure from the theoretical results. For example, for a sample of R_i= 2 and R_o=2, the applied pressure levels are consecutively 20 bar, 40 bar and 80 bar for a maximum allowable pressure level of 140 bar.

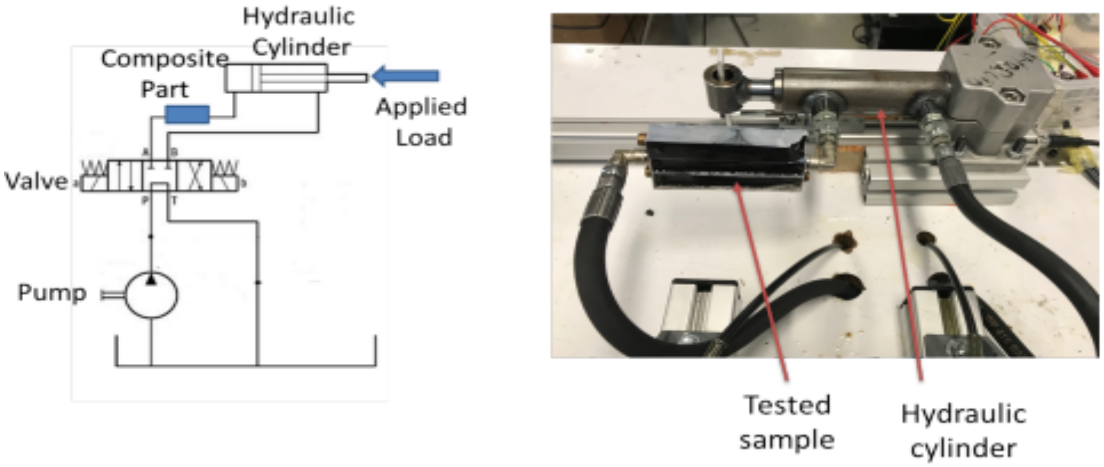

Fig. 12. Installation of the samples in a test bench and schematic presentation of the testing procedure

Then, the test is carried out and the pressure is measured using pressure sensors integrated at the inlet/outlet of the hydraulic cylinder. The obtained results are summarized in Figure 13. According to these measurements, the highest recorded pressure at failure for type 1 samples (R_i=1.5, R_o=2) is 50 bar while the lowest recorded pressure is 35 bar, while for type 2 (R_i=2, R_o=2) the highest recorded pressure is 120 bar while the lowest recorded pressure is 90 bar, both at a working flow rate of 12 L/min. Finally, for type 3 samples (R_i = 1.5, R_o=2) the highest recorded pressure is 75 bar while the lowest recorded pressure is 65 bar. These results validate the obtained theoretical results for an error which ranges from 6% for type 1 to 14% for type 3 samples. Consequently, the methodology is validated experimentally with a 90% average results coherence.

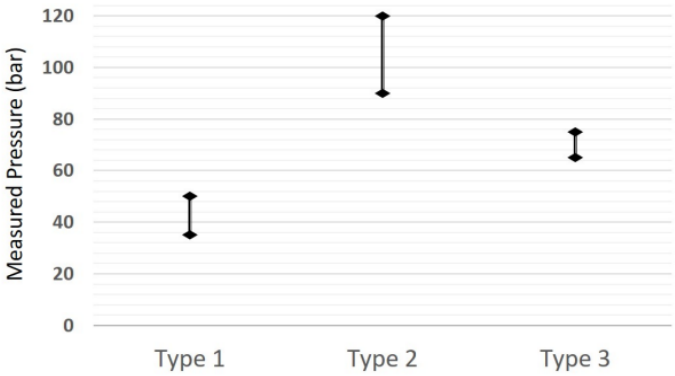

Fig. 13. Installation of the samples in a test bench and schematic presentation of the testing procedure

7. Conclusions and Future work

In this paper, a new methodology for fabricating hydraulic integrated mechanical components is presented and validated experimentally. The new methodology includes using silicon pipes for building the network of internal passages. Each network is built inside a 3D-printed mould which is designed accordingly. All the required hydraulic components are directly integrated into the printed mould. Then, a 3D-printed elbow is used to connect two perpendicular silicon pipes. A theoretical study is presented to define the design parameters and the working pressure at which the manufactured part can withstand. The design parameters that are studied are the internal diametric ratio Ri and the external diametric ratio Ro. The multi-layer theory is used where the internal layer is the silicone tube, while the external layer is a random fibre composite reinforcement. Next, a 3D model of a multilayer tube is built into FEM simulation software to verify the theoretical results. The obtained results give an overall average of 5% error between the theoretical and the FEM results. Additionally, these results are validated experimentally by hardware fabrication of 3 test samples, each of a different material category and they are tested in a hydraulic test bench with feedback pressure sensors. Hydraulic pressure is applied on these samples with a maximum allowable pressure of 140 bar and maximum flow of 12 L/min. The three samples were able to withstand the predefined applied pressure values. The experimental results are found to be as accurate as the theoretical model with 90% average results coherence.

Acknowledgement

This work is financially supported by the French company BIA- TURNKEY TEST SYSTEMS (BiA). The complete fieldwork has been done at the University of Versailles (UVSQ) - Paris Saclay, France.

References

[1] Laman, Edward, Mohd Nazmin Maslan, Mahasan Mat Ali, Lokman Abdullah, Ruzaidi Zamri, Mohd Syafiq Syed Mohamed, Maslan Zainon, Mohd Samsuddin Noorazizi, and Agus Sudianto. "Design of an Internet of Things Based Electromagnetic Robotic Arm for Pick and Place Applications." *Malaysian Journal on Composites Science and Manufacturing* 2, no. 1 (2020): 12-20. https://doi.org/10.37934/mjcsm.2.1.1220

[2] Nawawi, S. W., S. Sabikan, and O. Kanjou. "Q-parameterization control method for a class of two wheel mobile robot." *Journal of Advanced Research in Applied Mechanics* 27, no. 1 (2016): 1-15.

[3] Ahmad, Nur Irwany, Vernon Yeoh Sheng Liang, Diyya Hidayah Abd Rahman, Aimi Athirah Hazwani Zaidi, Saidatul Shema Saad, Nazrul Azril Nazlan, Habibah Mokhtaruddin, and Baseemah Mat Jalaluddin. "Development of Solar Tracking Robot for Improving Solar Photovoltaic (PV) Module Efficiency." *Journal of Advanced Research in Applied Mechanics* 61, no. 1 (2019): 13-24.

[4] Sukarman, Firdaus, Mohd Ghazali Mohd Hamami, Mazleenda Mazni, Muhammad Amir Mat Shah, and Ahmad Faidzal Khodori. "Parallelogram linkage leg structure for stabilized walking gaits in humanoid robot." *Journal of Advanced Research in Applied Sciences and Engineering Technology* 9, no. 1 (2017): 22-31.

[5] Massoud, Mostafa Mo, A. Abdellatif, and Mostafa RA Atia. "Different Path Planning Techniques for an Indoor Omni-Wheeled Mobile Robot: Experimental Implementation, Comparison and Optimization." *Applied Sciences* 12, no. 24 (2022): 12951. https://doi.org/10.3390/app122412951

[6] Asfour, Tamim, Lukas Kaul, Mirko Wächter, Simon Ottenhaus, Pascal Weiner, Samuel Rader, Raphael Grimm *et al.,* "Armar-6: A collaborative humanoid robot for industrial environments." In *2018 IEEE-RAS 18th International Conference on Humanoid Robots (Humanoids)*, pp. 447-454. IEEE, 2018. https://doi.org/10.1109/HUMANOIDS.2018.8624966

[7] Kaneko, Kenji, Hiroshi Kaminaga, Takeshi Sakaguchi, Shuuji Kajita, Mitsuharu Morisawa, Iori Kumagai, and Fumio Kanehiro. "Humanoid robot HRP-5P: An electrically actuated humanoid robot with high-power and wide-range joints." *IEEE Robotics and Automation Letters* 4, no. 2 (2019): 1431-1438. https://doi.org/10.1109/LRA.2019.2896465

[8] Bhattacharya, Sandip, Sunandan Dutta, Aiwen Luo, Mitiko Miura-Mattausch, Yoshihiro Ochi, and Hans Jürgen Mattausch. "Energy efficiency of force-sensor-controlled humanoid-robot walking on indoor surfaces." *IEEE Access* 8 (2020): 227100-227112. https://doi.org/10.1109/ACCESS.2020.3046279

[9] Sahekhaini, Asnizah, Norhayati Ibrahim, Bibie Sara Salleh, Salhana Sahidin, and Aminudin Abu. "Design of Multipurpose Hydraulic Tool for Door Installation." *Journal of Advanced Research in Applied Sciences and Engineering Technology* 19, no. 1 (2020): 1-5. https://doi.org/10.37934/araset.19.1.15

[10] Ibrahim, Ahmed Abdellatif Hamed, Stephanie Hallak, and Samer Alfayad. "Development of an on-board Power Pack for the hydraulic humanoid robot HYDROïD." *International Review of Mechanical Engineering (IREME)* 12, no. 8 (2018): 726. https://doi.org/10.15866/ireme.v12i8.14066

[11] Hirayama, Kenta, Nozomu Hirosawa, and Sang-Ho Hyon. "Passivity-based compliant walking on torque-controlled hydraulic biped robot." In *2018 IEEE-RAS 18th International Conference on Humanoid Robots (Humanoids)*, pp. 1-6. IEEE, 2018. https://doi.org/10.1109/HUMANOIDS.2018.8624964

[12] Dafarra, Stefano, Sylvain Bertrand, Robert J. Griffin, Giorgio Metta, Daniele Pucci, and Jerry Pratt. "Non-linear trajectory optimization for large step-ups: Application to the humanoid robot atlas." In *2020 IEEE/RSJ International Conference on Intelligent Robots and Systems (IROS)*, pp. 3884-3891. IEEE, 2020. https://doi.org/10.1109/IROS45743.2020.9341587

[13] Ibrahim, Ahmed Abdellatif Hamed, Anas Ammounah, Samer Alfayad, Sami Tliba, Fethi Ben Ouezdou, and Stéphane Delaplace. "Hydraulic Robotic Leg for HYDROïD Robot: Modeling and Control." *Journal of Robotics and Mechatronics* 34, no. 3 (2022): 576-587. https://doi.org/10.20965/jrm.2022.p0576

[14] Li, Xu, Songyuan Zhang, Haitao Zhou, Haibo Feng, and Yili Fu. "Locomotion adaption for hydraulic humanoid wheel-legged robots over rough terrains." *International Journal of Humanoid Robotics* 18, no. 01 (2021): 2150001. https://doi.org/10.1142/S0219843621500018

[15] Sahu, Govind N., Suyash Singh, Aditya Singh, and Mohit Law. "Static and dynamic characterization and control of a high-performance electro-hydraulic actuator." In *Actuators*, vol. 9, no. 2, p. 46. MDPI, 2020. https://doi.org/10.3390/act9020046

[16] Semini, Claudio, Nikos G. Tsagarakis, Emanuele Guglielmino, and Darwin G. Caldwell. "Design and experimental evaluation of the hydraulically actuated prototype leg of the HyQ robot." In *2010 IEEE/RSJ International Conference on Intelligent Robots and Systems*, pp. 3640-3645. IEEE, 2010. https://doi.org/10.1109/IROS.2010.5651548

[17] Elasswad, M., A. Tayba, A. Abdellatif, S. Alfayad, and K. Khalil. "Development of lightweight hydraulic cylinder for humanoid robots applications." *Proceedings of the Institution of Mechanical Engineers, Part C: Journal of Mechanical Engineering Science* 232, no. 18 (2018): 3351-3364. https://doi.org/10.1177/0954406217731794

[18] Amrollah, Elmira, A. Abdellatif, Samer Alfayad, and Féthi Ben Ouezdou. "Performance enhancement of an integrated electro-hydraulic actuator using dynamic modeling and optimization." *Proceedings of the Institution of Mechanical Engineers, Part C: Journal of Mechanical Engineering Science* 237, no. 12 (2023): 2815-2832. https://doi.org/10.1177/09544062221142404

[19] Saeedvand, Saeed, Masoumeh Jafari, Hadi S. Aghdasi, and Jacky Baltes. "A comprehensive survey on humanoid robot development." *The Knowledge Engineering Review* 34 (2019): e20. https://doi.org/10.1017/S0269888919000158

[20] Barasuol, Victor, Octavio A. Villarreal-Magaña, Dhinesh Sangiah, Marco Frigerio, Mike Baker, Robert Morgan, Gustavo A. Medrano-Cerda, Darwin Gordon Caldwell, and Claudio Semini. "Highly-integrated hydraulic smart actuators and smart manifolds for high-bandwidth force control." *Frontiers in Robotics and AI* 5 (2018): 51. https://doi.org/10.3389/frobt.2018.00051

[21] Semini, Claudio, Jake Goldsmith, Diego Manfredi, Flaviana Calignano, Elisa Paola Ambrosio, Jukka Pakkanen, and Darwin G. Caldwell. "Additive manufacturing for agile legged robots with hydraulic actuation." In *2015 International Conference on Advanced Robotics (ICAR)*, pp. 123-129. IEEE, 2015. https://doi.org/10.1109/ICAR.2015.7251444

[22] Sun, Maowen, Xiaoping Ouyang, Jouni Mattila, Huayong Yang, and Gang Hou. "One novel hydraulic actuating system for the lower-body exoskeleton." *Chinese Journal of Mechanical Engineering* 34 (2021): 1-10. https://doi.org/10.1186/s10033-021-00535-w

[23] Lee, Dongyoung, Buchun Song, Sang Yong Park, and Yoon Su Baek. "Development and control of an electro-hydraulic actuator system for an exoskeleton robot." *Applied Sciences* 9, no. 20 (2019): 4295. https://doi.org/10.3390/app9204295

[24] Dutta, Varun, Sanjay Sharma, Kapil Chopra, and Balbir Singh. "Hybrid electric discharge machining processes for hard materials: a review." *Materials Focus* 5, no. 3 (2016): 202-208. https://doi.org/10.1166/mat.2016.1361

[25] Abdulhameed, Osama, Abdulrahman Al-Ahmari, Wadea Ameen, and Syed Hammad Mian. "Additive manufacturing: Challenges, trends, and applications." *Advances in Mechanical Engineering* 11, no. 2 (2019): 1687814018822880. https://doi.org/10.1177/1687814018822880

[26] Ganachari, Vaibhav, Uday Chate, Laxman Waghmode, Prashant Jadhav, Satish Mullya, and Prasad. "Simulation and experimental investigation of performance characteristics of dry and near dry EDM process." *Advances in Materials and Processing Technologies* 8, no. 3 (2022): 3013-3028. https://doi.org/10.1080/2374068X.2021.1945296

[27] Banu, Asfana, and Mohammad Yeakub Ali. "Electrical discharge machining (EDM): a review." *International Journal of Engineering Materials and Manufacture* 1, no. 1 (2016): 3-10. https://doi.org/10.26776/ijemm.01.01.2016.02

[28] Evjemo, Linn Danielsen, Signe Moe, Jan Tommy Gravdahl, Olivier Roulet-Dubonnet, Lars Tore Gellein, and Vegard Br. "Additive manufacturing by robot manipulator: An overview of the state-of-the-art and proof-of-concept results." In *2017 22nd IEEE International Conference on Emerging Technologies and Factory Automation (ETFA)*, pp. 1-8. IEEE, 2017.

[29] Bhavar, Valmik, Prakash Kattire, Vinaykumar Patil, Shreyans Khot, Kiran Gujar, and Rajkumar Singh. "A review on powder bed fusion technology of metal additive manufacturing." *Additive manufacturing handbook* (2017): 251-253. https://doi.org/10.1201/9781315119106-15

[30] Jiang, Zhongyu, Yajun Zhang, Huaqing Liu, and Xuanxuan Li. "Symplectic Elastic Solution of Multi-layer Thick-Walled Cylinder Under Different Interlayer Constraints." In *International Conference on Civil Engineering*, pp. 238-253. Singapore: Springer Singapore, 2021. https://doi.org/10.1007/978-981-19-1260-3_21

[31] Hutař, P., M. Zouhar, L. Náhlík, M. Ševčík, and B. Máša. "Multilayer polymer pipes failure assessment based on a fracture mechanics approach." *Engineering Failure Analysis* 33 (2013): 151-162. https://doi.org/10.1016/j.engfailanal.2013.04.022